Electronic Supplementary Material (ESI) for Nanoscale.

Supplementary Information: Phase control and lateral heterostructures of $MoTe_2$ epitaxially grown on graphene/Ir(111)

Joan Ripoll-Sau[a,b], **Fabian Calleja**[a], **Pablo Casado Aguilar**[a,b], **Iván M. Ibarburu**[a,b], **Amadeo L. Vázquez de Parga**[a,b,c,d], **Rodolfo Miranda**[a,b,c,d], **Manuela Garnica**[a,c]

[a] Instituto Madrileño de Estudios Avanzados en Nanociencia (IMDEA-Nanociencia), 28049 Madrid, Spain
[b] Departamento de Física de la Materia Condensada, Universidad Autónoma de Madrid, 28049 Madrid, Spain
[c] Instituto "Nicolás Cabrera", Universidad Autónoma de Madrid, 28049 Madrid, Spain
[d] Condensed Matter Physics Center (IFIMAC), Universidad Autónoma de Madrid, 28049 Madrid, Spain

E-mail: `manuela.garnica@imdea.org`

1. Role of the Te:Mo ratio in the growth of 2D-$MoTe_2$ and nanowires

Two different approaches have been explored to study the influence of the Te:Mo ratio in the $MoTe_2$ growth: (i) The Te effective flux was increased by varying the number of operative Knudsen cells (from 1 to 3) at a given cell temperature and (ii) the $Flux_{Mo}$ was increased while the T_{sample} and exposure time were set.

Figure S1 shows a series of STM images taken on three different samples prepared by exposing the substrate at fixed T_{sample}=500 K and $Flux_{Mo}$=60 nA, while the Te exposure was increased by varying the number of operative Knudsen cells from (a) one, (b) two or (c) three, respectively. A clear dependence on the Te exposure can be observed.

At the lowest Te:Mo ratio (4:1), Fig. S1(a), the $MoTe_2$ islands cover only a $21 \pm 2\%$ of the surface while $39 \pm 2\%$ of the surface presents elongated structures. When the Te:Mo ratio is increased to 8:1 by opening a second Te cell, see Fig. S1(b), we recognize well-defined $MoTe_2$ islands, as their coverage rises to $42 \pm 4\%$ and the wires population is reduced to $9 \pm 1\%$. It is necessary to open the third Te cell and slightly increase the T_{Te} temperature to 610 K, which corresponds to a Te:Mo flux ratio around 12:1, in order to produce large islands with the appropriate $MoTe_2$ stoichiometry, see Fig. S1(c). Under these conditions, the $MoTe_2$ islands increase considerably in size and cover the $49 \pm 2\%$ of the surface. The sequence presented here indicates that a proper $MoTe_2$ growth requires Te saturation conditions to prevent the many Te-deficient phases discussed above.

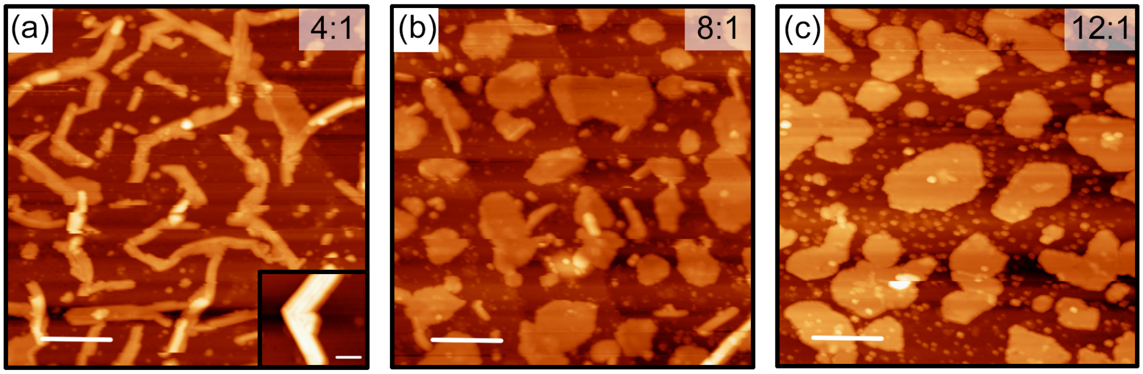

Figure S1: STM images showing the evolution of the $MoTe_2$ growth with increasing Te flux. The growth was performed under a constant flux of Mo ($\mathrm{Flux}_{\mathrm{Mo}}$=60 nA), a T_{sample}=500 K and with (a) one (4:1), (b) two (8:1) or (c) three cells (12:1) of the Te evaporator at T_{Te}=600-610K. The images were taken at RT and (a) $V_b = 2\,\mathrm{V}$ and $I_t = 0.3\,\mathrm{nA}$, (b) $V_b = 2\,\mathrm{V}$ and $I_t = 0.3\,\mathrm{nA}$ and (c) $V_b = -1\,\mathrm{V}$ and $I_t = 0.3\,\mathrm{nA}$. The corresponding scale bars are 20 nm. A close view of one of the Mo_6Te_6 multiwire structure is shown in the inset of (a), where the scale bar is 4 nm.

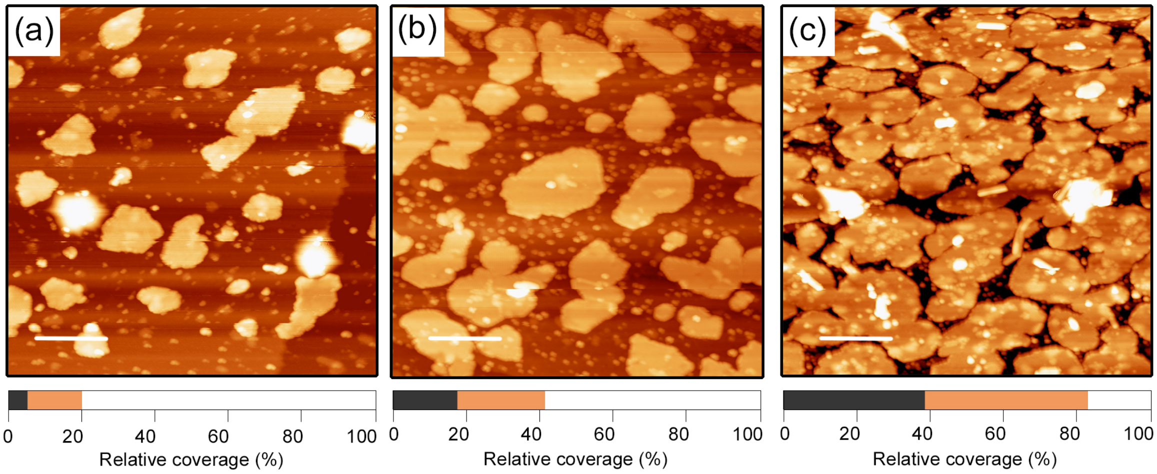

Figure S2: Series of STM images showing the evolution of the $MoTe_2$ growth with increasing the Mo flux. The growth was performed under a constant flux of Te (three cells at T_{Te}=610 K), a sample temperature of 500 K and a Mo flux of (a) 20 nA, (b) 60 nA and (c) 150 nA. The barplots display the relative coverage of 1H (black) and 1T' (orange) phases. All images were taken at RT with $V_b = 2\,\mathrm{V}$ and $I_t = 0.3\,\mathrm{nA}$. The scale bars are 20 nm.

In order to confirm this point, the evolution of the $MoTe_2$ growth with the $Flux_{Mo}$ was also investigated, as shown in Figure S2. Accordingly, the $Flux_{Mo}$ was increased while the substrate was held at T_{sample}=500 K and Te exposure was fixed to three cells at T_{Te}=610 K to ensure Te saturation conditions. Growth time was fixed to 30 min. At first glance, we can see how the $MoTe_2$ coverage increases going from 20 ± 2%, 42 ± 3% to 83 ± 1% and more importantly, no trace of the Te-deficient structures discussed above is found. This fact evidences that the real limiting factor during the reaction in this case is Mo. In addition, careful inspection of the islands allows us to explore how the 1H:1T´ ratio varies as the amount of Mo is increased. This can be seen in the lower panels of Fig. S2, where barplot representations of the relative coverage of 1H and 1T' phases is pictured in black and orange color, respectively. Whereas for high Te:Mo ratio, Fig. S2(a), the formation of the 1T' phase is promoted, for lower Te:Mo ratios, the relative coverage of 1H and 1T' phases balances, as shown by the barplots of Fig. S2(b) and S2(c). This indicates that the excess of Te promotes the growth of the 1H phase.

2. 2D-$MoTe_2$ phases

Figure S3(a) shows a large scale STM image after exposing the gr/Ir(111) surface at T_{sample}=500 K to a Te:Mo ratio of 10.

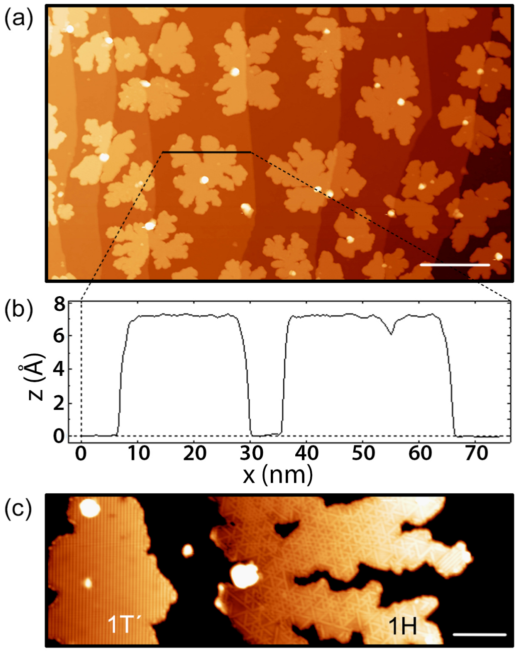

Figure S3: (a) Large scale STM image of $MoTe_2$ grown on gr/Ir(111) (V_b = 1 V and I_t = 0.1 nA, scale bar 60 nm) and (b) height profile along the black line shown in (a). (c) Closer view of a 1H and a 1T' islands (V_b = 1 V and I_t = 0.1 nA, scale bar 20 nm). Measurements were performed at 1.2 K.

The average STM apparent height of the islands in the imaging conditions of the figure is 7.2 ± 0.1Å, as shown in the profile (Fig. S3(b)) taken along the black line indicated in Fig. S3(a). This value indicates that the islands are a Te-Mo-Te trilayer high, the value being slightly larger than c=6.20 Å measured by diffraction in a $MoTe_2$ bulk crystal [1], but in agreement with the values reported by STM for $MoTe_2$ monolayers on different substrates [2, 3, 4]. A closer view of the islands, see Fig. S3(c), reveals the presence of two different types of surface structures, which can either encompass complete islands or be present adjacent to each other in the same island. Based on their structure, we identify them with the two stable polytype structures of $MoTe_2$: the 1H and 1T' phases, see Fig. S4.

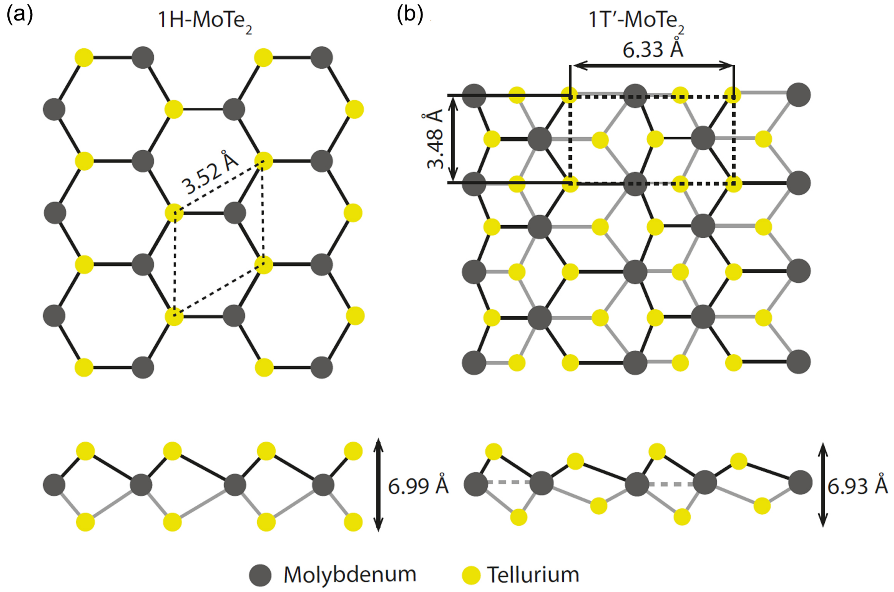

Figure S4: Models of the (a) trigonal prismatic 1H-$MoTe_2$ structure and (b) distorted octahedral 1T'-$MoTe_2$ and their corresponding lattice parameters extracted from X-ray diffraction experiments [5].

In $MoTe_2$, the Mo atom is 6-fold coordinated by chalcogens, assuming two possible structural polytypes [6]: the semiconducting trigonal prismatic phase (2H in bulk crystals and 1H at the monolayer regime) and the distorted semimetallic octahedral prismatic phase (1T'). A model of both structures in 2D, together with their lattice parameters extracted from X-ray diffraction measurements [5] is shown in Fig. S4.

3. Preferential orientation of 1T'-$MoTe_2$ islands

After the growth of $MoTe_2$ on gr/Ir(111), our STM images reveal that the 1T'-$MoTe_2$ islands are preferentially oriented. In order to quantify this observation, we measured the relative orientation of the stripes of the 1T' islands before (black) and after (blue) a post-annealing.

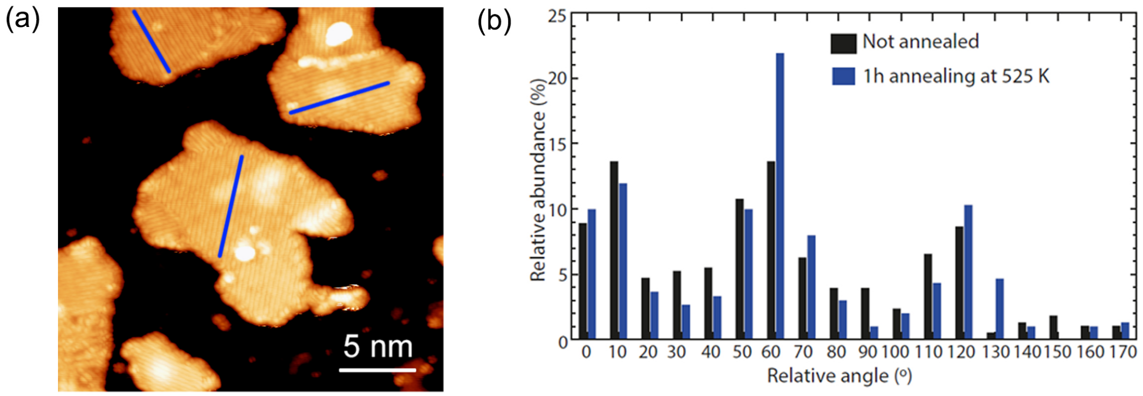

Figure S5: (a) STM image after the growth of $MoTe_2$ ($V_\mathrm{b} = 1\,\mathrm{V}$ and $I_\mathrm{t} = 0.1\,\mathrm{nA}$). (b) Bar graph comparing the relative angle between 1T´-$MoTe_2$ islands before (black) and after (blue) post annealing the sample at 520 K for 1h. Measurements performed at 1.2 K.

As can be seen in Figure S5, three orientations separated by nearly 60º are clearly favored, as expected for a two-fold symmetric structure on top of a six-fold symmetric substrate as graphene. Interestingly, after the post-annealing for 1 h the abundance of the highly oriented islands increase, indicating the benefits of annealing in terms of epitaxy.

4. New polymorph phase: $v1$H-Mo_5Te_8

Under Mo-rich conditions, it is common to find areas exhibiting different voltage-dependent structures embedded inside 1H-$MoTe_2$ islands. We identified these areas with a new polymorphic phase of $MoTe_2$ reported by Zhang and co-workers [7], named v1H-Mo_5Te_8. A model of this new phase is shown in Fig. S6.

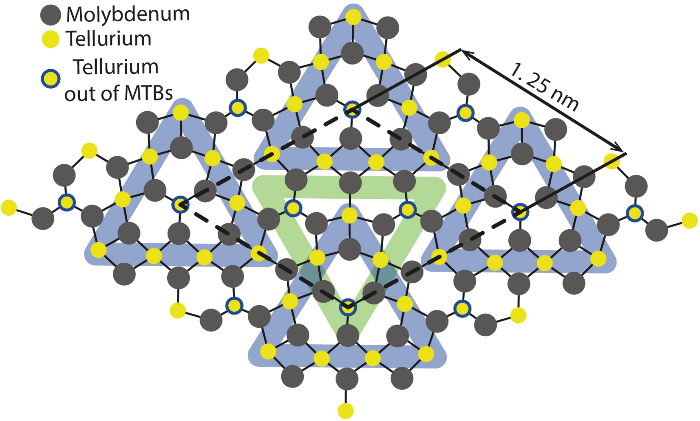

Figure S6: Model of the v1H-Mo_5Te_8 phase based in ref [7]. The unit cell is marked with a dashed black rhombus. The MTB loops and the area between them are highlighted in blue and green, respectively.

A series of STM images at different bias voltages from 2 V to −2 V were taken and classified according to the observed structure, as shown in Fig. S7. Even though we distinguish nine different structures, their periodicities can be reduced to 0.71 nm between (−2 V,−0.5 V) and (1.2 V, 2 V) and 1.25 nm between (−0.5 V, 1.2 V). Interestingly, an inversion of the contrast also occurs between positive and negative voltages in the 0.71 nm periodic structure.

In order to clarify the origin of the bias-dependent patterns, we studied the spatial modulation of the LDOS in these areas. Figure S8 (a), (b) and (c) shows dI/dV images taken at the same position in a different area at 60 mV, 260 mV and 1 V, respectively. The dI/dV image taken at 60 mV shows a periodic distribution of dark areas matching the periodicity of the 1.25 nm, see blue squares in Fig. S8 (a), surrounding of bright protrusions highlighted with red and green squares. At 260 mV, the three areas mentioned before are found as bright features. Finally, in the dI/dV image at 1 V (Fig. S8 (c)) a triangular structure with a bright center can be resolved. Individual STS curves were extracted from the CITS in the most representative areas marked by colored squares in Figure S8 (a), (b) and (c). As can be observed, the 50 mV peak is more intense in the red and green areas, which have a higher density of Mo atoms. Conversely, the Te atom at the center of the MTB loop in Fig. S6 presents a larger contribution to the 250 mV peak.

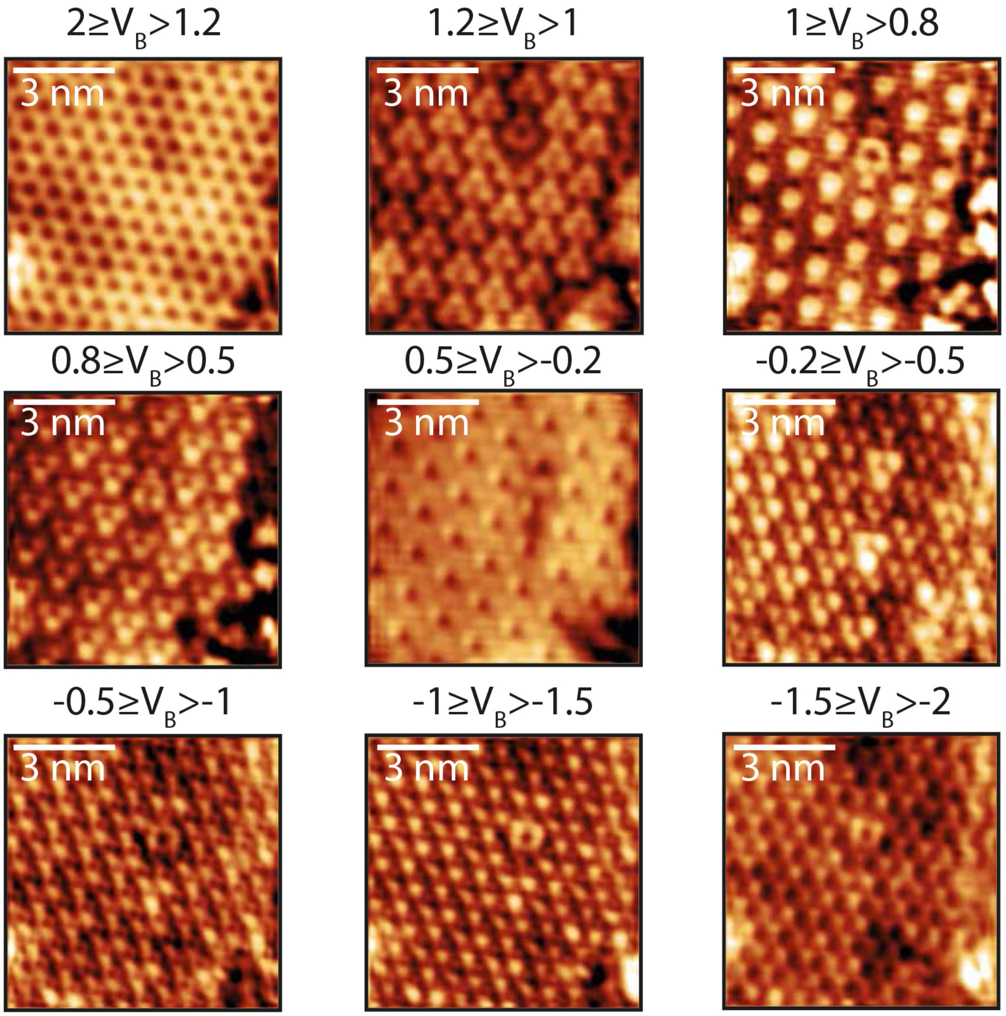

Figure S7: Series of STM images on a single domain of the v1H-Mo_5Te_8 phase at different bias voltage. Images were taken at 1.2 K and $I_t = 0.1\,nA$ varying from 2 V to $-2\,V$ in 0.1 voltage steps.

In conclusion, on the one side, the 1.25 nm hexagonal structure is originated either by the MTBs loops highlighted in blue in Fig. S6 or by the area between the MTB loops highlighted in green. On the other hand, the 0.71 nm structure is produced by those Te atoms that do not belong to any MTB, marked in Fig. S6 by yellow circles with blue perimeter.

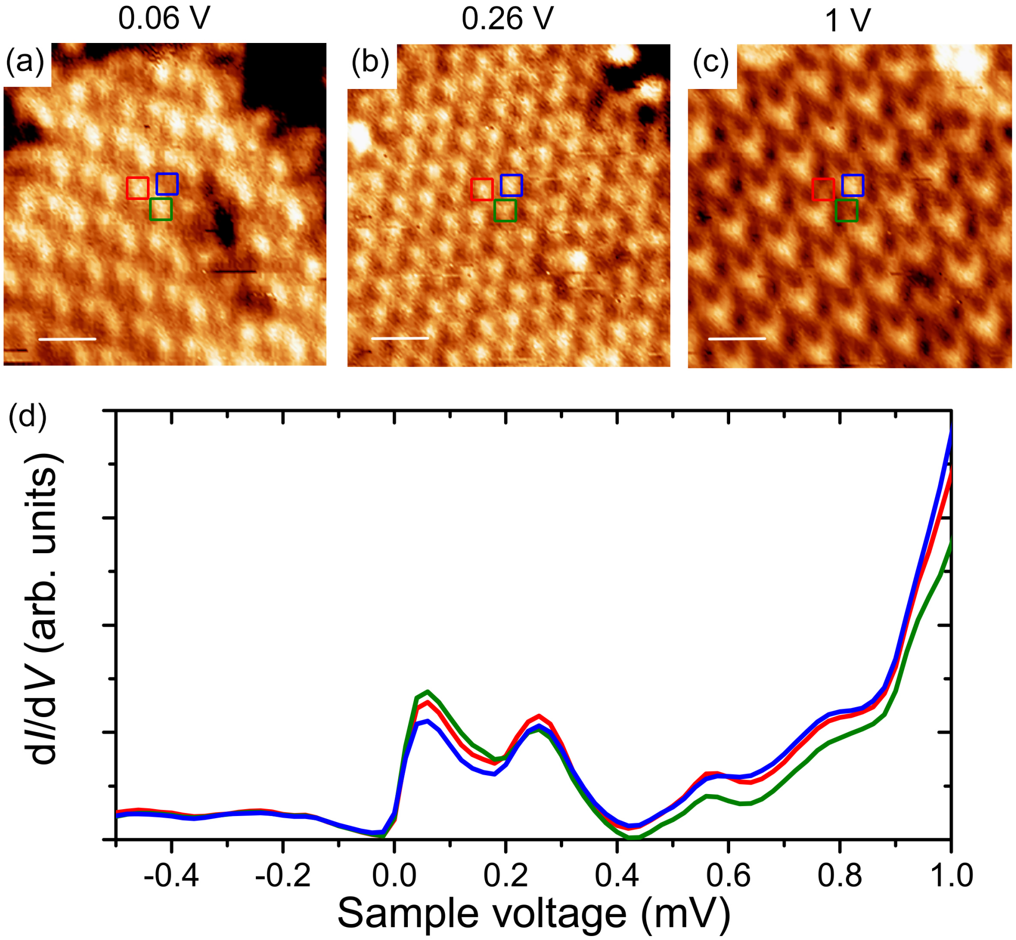

Figure S8: Modulation of the v1H-Mo_5Te_8 electronic structure. (a), (b) and (c) dI/dV images extracted from a CITS ($V_b = 1\,V$ and $I_t = 1\,nA$ and $V_{mod} = 20\,mV$) at 60 mV, 260 mV and 1 V respectively. (d) STS curve extracted from the square areas marked areas in (a), (b) and (c). Measurements performed at T=1.2 K.

5. Mirror Twin Boundaries

We identify the MTBs of $MoTe_2$ with the 4—4P-type Mo-rich MTBs, see Fig. S9(b), in which a row of Te atoms is shared between two 1H domains rotated 60°. Our low-temperature scanning tunnelling microscopy/spectroscopy measurements revealed the presence of an energy gap opening at the Fermi energy. We find that the gap size changes from one to another MTB, varying from 35 to 65 meV, but remains constant along the same MTB. We attribute this behaviour to the formation of a charge density wave (CDW) along the 1D defects [8, 9].

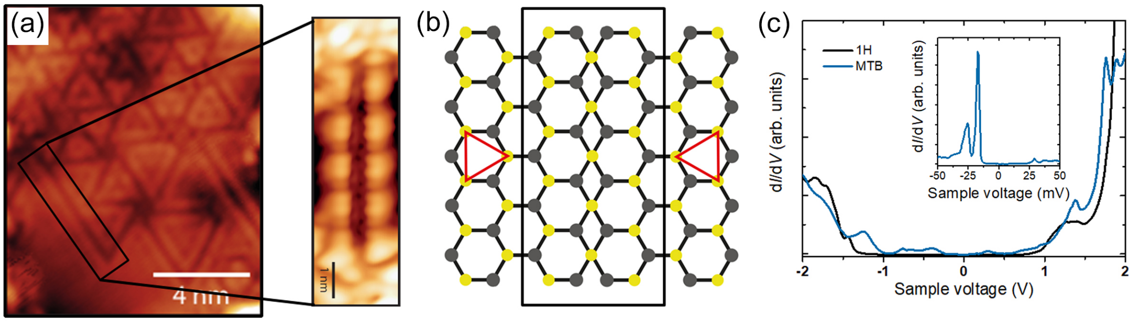

Figure S9: Structural and electronic properties of the MTBs. (a) STM image of a 1H-MoTe$_2$ region ($V_\mathrm{b} = -1\,\mathrm{V}$ and $I_\mathrm{t} = 0.1\,\mathrm{nA}$) and a zoom of a MTB ($V_\mathrm{b} = -0.35\,\mathrm{V}$ and $I_\mathrm{t} = 1\,\mathrm{nA}$). (b) Model of the MTB where the grey and yellow circles represent Mo and Te atoms, respectively. (c) Average spectrum taken at the MTB (blue) and compared to the one taken in a defect free 1H area. The inset shows a spectrum taken with higher energy resolution in a narrower energy window ($V_\mathrm{mod} = 400\mu\,\mathrm{V}$) showing the characteristic gap of the MTB.

References

[1] Puotinen D and Newnham R E 1961 *Acta Crystallographica* **14** 691–692

[2] Chen J, Wang G, Tang Y, Tian H, Xu J, Dai X, Xu H, Jia J, Ho W and Xie M 2017 *ACS Nano* **11** 3282–3288

[3] Yu Y, Wang G, Qin S, Wu N, Wang Z, He K and Zhang X A 2017 *Carbon* **115** 526–531

[4] Yu Y, Wang G, Tan Y, Wu N, Zhang X A and Qin S 2018 *Nano Letters* **18** 675–681

[5] Vishwanath S, Sundar A, Liu X, Azcatl A, Lochocki E, Woll A R, Rouvimov S, Hwang W S, Lu N, Peng X, Lien H H, Weisenberger J, McDonnell S, Kim M J, Dobrowolska M, Furdyna J K, Shen K, Wallace R M, Jena D and Xing H G 2018 *Journal of Crystal Growth* **482** 61–69

[6] Sokolikova M S and Mattevi C 2020 *Chemical Society Reviews* **49** 3952–3980

[7] Zhang J, Xia Y, Wang B, Jin Y, Tian H, kin Ho W, Xu H, Jin C and Xie M 2021 *2D Materials* **8** 015006

[8] Wang L, Wu Y, Yu Y, Chen A, Li H, Ren W, Lu S, Ding S, Yang H, Xue Q K, Li F S and Wang G 2020 *ACS Nano* **14** 8299–8306

[9] Batzill M 2018 *Journal of Physics Condensed Matter* **30** 493001